A Fuzzy Hierarchical Strategy for Improving Frequency Regulation of Battery Energy Storage System

Kaifeng Wang, Ying Qiao, Lirong Xie, Jiaming Li, Zongxiang Lu, and Huan Yang

Abstract—Battery energy storage systems (BESSs) can provide instantaneous support for frequency regulation (FR) because of their fast response characteristics. However, purely pursuing a better FR effect calls for continually rapid cycles of BESSs, which shortens their lifetime and deteriorates the operational economy. To coordinate the lifespan savings and the FR effect, this paper presents a control strategy for the FR of BESSs based on fuzzy logic and hierarchical controllers. The fuzzy logic controller improves the effect of FR by adjusting the charging/discharging power of the BESS with a higher response speed and precision based on the area control error (ACE) signal and the change rate of ACE in a non-linear way. Hierarchical controllers effectively reduce the life loss by optimizing the depth of discharge, which ensures that the state of charge (SOC) of BESS is always in the optimal operating range, and the total FR cost is the lowest at this time. The proposed method can achieve the optimal balance between ACE reduction and operational economy of BESS. The effectiveness of the proposed strategy is verified in a two-area power system.

Index Terms—Battery energy storage system (BESS), frequency regulation (FR), coordinated control strategy, optimal depth of discharge, charging/discharging threshold.

NOMENCLATURE

A. Variables

$\alpha_1, \alpha_2, \varepsilon, \gamma, \phi, \mu$	Custom parameters
β	Capacity conversion coefficient
γ	Penalty coefficient
η_c, η_{disc}	Charging and discharging efficiencies of battery energy storage system (BESS)
δ	Fitting coefficient
ACE	Area control error (ACE)
$A\dot{C}E$	ACE change rate
ACE_F	ACE signal output by fuzzy logic controller
ACE_F^{dz}	Response threshold of frequency regulation (FR) dead zone
ACE_E^c, ACE_E^{disc}	Response charging and discharging power value of sub-BESS
ACE_F^{em}	Response thresholds of FR emergency zone
B	Bias factor
B_{con}	Throughput conversion times
c	Custom parameter
C_E	BESS capacity
D	Load-damping coefficient
Δf	Frequency deviation
F_{HP}	High pressure power fraction of reheat turbine
F_{cost}	FR cost
$G_E(s)$	Transfer function of BESS
$G_g(s)$	Transfer function of conventional unit
M	System inertia constant
K_E	BESS gain
K_P, K_I	Coefficients of proportional and integral controllers
L_{life}	Cycle times of BESS
L_{loss}	Total life loss during entire FR process
N	Cycle times under 100% depth of discharge (DOD)
P_E	BESS power
ΔP_E	Power change of BESS
$\Delta P_E^c, \Delta P_E^{disc}$	Charging and discharging power of BESS
$\Delta P_{E,ACE}^c, \Delta P_{E,ACE}^{disc}$	Charging and discharging power of BESS based on ACE
$P_{E,\,max}$	The maximum throughput power of BESS
$P_{E,\,max}^c, P_{E,\,max}^{disc}$	The maximum charging and discharging power of BESS

K. Wang, L. Xie (corresponding author), and H. Yang are with the School of Electrical Engineering, Xinjiang University, Urumqi, China (e-mail: 861554820@qq.com; 541391018@qq.com; 1020443726@qq.com).

Y. Qiao, J. Li, and Z. Lu are with the State Key Laboratory of Control and Simulation of Power Systems and Generation Equipments of Electrical Engineering, Tsinghua University, Beijing, China (e-mail: qiaoying@tsinghua.edu.cn; lijiaminggood@163.com; luzongxiang98@mail.tsinghua. edu.cn).

$\Delta P_{E,r}^{c}$, $\Delta P_{E,r}^{disc}$	Realistic charging and discharging power of BESS
ΔP_L	Load fluctuation
R	Difference coefficient
SOC	State of charge (SOC) of BESS
$SOC_{initial}$	Initial value of SOC
SOC_{low}, SOC_{high}	The low and high values of SOC
SOC_{min}, SOC_{max}	The minimum and maximum values of SOC
T_{CH}	Time constant of steam chest
T_E	Time constant of BESS
T_{RH}	Time constant of reheat turbine
T_{tie}	Delay constant of two areas
u	BESS utilization
w_P	Power cost of BESS
w_E	Capacity cost of BESS
W	Total construction cost of BESS, and $W = w_P P_E + w_E C_E$

B. Subscript and Superscript

c, $disc$	Charging and discharging
1, 2	Sub-BESS 1 and sub-BESS 2

I. Introduction

THE development of renewable energy sources raises a series of problems in maintaining the balance between the power production and demand [1]-[3]. Multiple frequency safety accidents indicate that the power system with a high penetration rate of renewable energy requires a fast and stable frequency regulation (FR) resource, which can provide considerable active power support at the early frequency change stage [4]. The fast response and customized parameters make battery energy storage system (BESS) an excellent FR resource [5], [6]. However, the expensive cost and repeated charging/discharging would limit the ability to provide a large amount of active power [7], [8]. It has become a research hotpot to find ways to improve the control strategy, enhance the FR effect, and decrease the cost.

To track the power gaps accurately, the BESS needs a proper strategy to respond to frequency changes. The commonly-used control strategies are virtual droop control and virtual inertia control [9], [10]. A virtual inertia emulator-based model predictive control is used to allow BESS to participate in FR [11], [12]. The above strategies enhance the FR effect by responding to the frequency signal, while a related study shows that the frequency deviation can be reduced by controlling the throughput of the BESS-based area control error (ACE) or area regulation requirement [13]. These research works provide good control methods, but they cannot accurately track the ACE signal and do not consider the life loss of BESS. In [14] and [15], some coordinated control strategies are proposed to support FR by controlling the operation of wind power and BESS. However, the

frequency signal changes continually and quickly, which causes repetition and control delay, and the control strategies cannot achieve the desired effect.

To solve this problem, heuristic-based controllers, such as fuzzy logic controller, have been proposed as an effective FR method. Different from the control strategies that consider a single frequency variable, the fuzzy logic controller has multiple inputs. It can control the BESS power by considering multiple variables related to the frequency and responds quickly to the ACE signal, which combines the advantages of conventional control methods such as inertial control and droop control. After passing the fuzzy logic controller, the frequency change signals become more precise, which helps the BESS respond to power demands more quickly in a complex power system [16]. However, these control methods focus more on the throughput power of BESS and cannot accurately control the state of charge (SOC). The SOC has a significant impact on the benefits and life loss of BESS. Therefore, the SOC recovery control must be considered in FR [17]. Related studies note that the deep charging/discharging of BESS can be reduced by using an SOC recovery strategy in the dead zone, which prolongs the BESS lifespan [18], [19]. In addition, recent studies further analyze the control strategy of hybrid energy storage and electric vehicles (EVs) participating in FR by BESS with an SOC recovery strategy [20] - [22]. Some studies propose using supercapacitors or EVs with BESSs to participate in FR through a coordinated control strategy [23], [24]. The above strategies have improved the FR effect. The grid-connected hybrid energy storage and EVs have the capacity to provide additional active power to the power system, which can be an alternative to the FR of BESS by EVs. However, the above strategy does not consider the controllability of EVs connected to grid, which cannot guarantee that EVs respond to the power demand in time, which is an ideal scenario from the current situation. References [25] and [26] focus on the integrated control between heuristic-based controllers and self-adaptive modification of SOC, which enhance the FR effect and improve the SOC health but cannot solve the contradiction between the FR effect and cost.

All the research achievements reported in the above papers either analyze the FR effect of BESS or the SOC recovery strategies. However, the studies mentioned above do not consider these goals together. The factor most directly related to the FR cost is the life loss of energy storage. Some studies have investigated the relationship between the depth of discharge (DOD) and the lifespan of BESS [27]. However, this paper is based on the BESS characteristics to test the cycle life and does not mention the FR risk to the system. In [28] and [29], the SOC of BESS is determined through the economic evaluation of cycle life, but the reference factor does not include the economic loss caused by the ACE deviation. In [30] and [31], some evaluation methods are proposed for BESSs in FR considering power loss, effectiveness, cycle number and other factors. In addition, the FR cost can be reduced through the SOC management of BESS [32]. However, these studies do not optimize the DOD of

BESS in FR.

In summary, the FR in modern power system faces the contradiction between the FR effect and the life loss of BESS. Shallow charging/discharging is beneficial to prolong the service life of BESS, but to improve the FR effect, the BESS needs to be charged and discharged deeply when the power shortage is large, which increases the life loss. A strategy is needed to improve the FR effect and reduce the life loss of BESS at the same time. The contribution of this paper is that a novel coordinated FR control strategy based on the fuzzy logic and hierarchical controllers to improve the power system stability is proposed. The fuzzy logic controller improves the FR effect by tracking the signal with a higher response speed and precision. The hierarchical controller reduces repeated charging/discharging of BESS. Through optimizing the DOD, the SOC of BESS is always in the optimal operating range, and the total FR cost is the lowest at this time, which reduces the life loss of BESS. Finally, the optimal DOD is given based on the influence of multiple parameters on the FR cost.

The remainder of this paper is organized as follows. Section II presents a comprehensive introduction to the FR model proposed in this paper, and a novel coordinated FR control strategy based on fuzzy logic and hierarchical controllers is presented. Section III introduces a comprehensive evaluation method for the FR effect with BESS. The simulation results are given and discussed in Section IV. Finally, Section V concludes this paper.

II. COORDINATED BESS CONTROL STRATEGY

A. FR Model

This sector discusses the coordinated BESS control strategy, i.e., BESS's instantaneous responses to power system ACE signals. The whole coordinated control strategy includes three parts: the fuzzy logic controller, hierarchical control strategy, and SOC limiter. A two-area system model is used for the conventional unit and BESS participating in FR, as shown in Fig. 1.
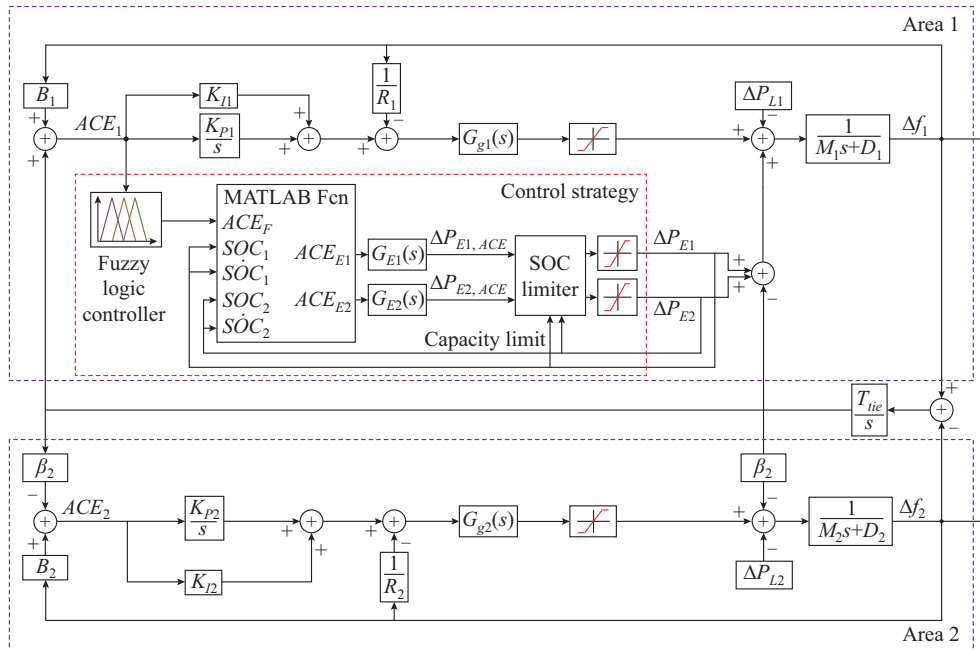

Fig. 1.   Diagram of two-area system model.

Different from conventional units, BESSs enable the responses to frequency fluctuations and supply a sizable amount of active power within one second. Through the appropriate control, BESSs can be used as outstanding resources to provide FR services. As shown in Fig. 1, the basic principle of BESS participating in FR is that BESS reasonably charges and discharges by tracking the change in the ACE. The transfer function of BESS is modeled as:

$$\Delta P_E(s) = \Delta ACE \cdot G_E(s) \tag{1}$$

$$G_E(s) = \frac{K_E}{1 + sT_E} \tag{2}$$

The rapid response of the BESS prevents further frequen-

cy deterioration in the power system. However, the throughput power of BESS is also limited as:

$$-P_{E,\max} < \Delta P_E < P_{E,\max} \tag{3}$$

The BESS receives the value of ΔP_E calculated by the throughput efficiency as follows:

$$\begin{cases} \Delta P_{E,r}^c = \eta_c \Delta P_E^c \\ \Delta P_{E,r}^{disc} = \dfrac{\Delta P_E^{disc}}{\eta_{disc}} \end{cases} \tag{4}$$

In addition to the throughput power and efficiency constraints, the BESS operation is also subject to the SOC. The SOC of BESS depends on the nominal capacity and power, and is defined as:

$$SOC = \left(SOC_{initial} + \frac{\int \Delta P_{E,r}^{c/disc} \, dt}{C_E}\right) \times 100\% \tag{5}$$

$$SOC_{min} < SOC < SOC_{max} \tag{6}$$

B. Fuzzy Logic Controller

When the power system frequency deteriorates, the ACE signals are transmitted to the FR resources.

The fuzzy logic controller designed in this paper has two inputs and one output. One input is the ACE signal, and the other input is $A\dot{C}E$. The output is ACE_F, which is the reference value of the BESS charging/discharging power through a fuzzy logic controller. Based on the ACE signals, the output of fuzzy logic controller considers the ACE change rate. The fuzzy logic controller adopts a Mamdani-type membership function. The inputs and output fuzzy sets are described as negative big (NB), negative medium (NM), negative small (NS), zero (Z), positive small (PS), positive medium (PM), and positive big (PB). The fuzzy logic rules are presented in Table I, and the membership functions of the inputs and output are shown in Fig. 2.

TABLE I
FUZZY LOGIC RULES

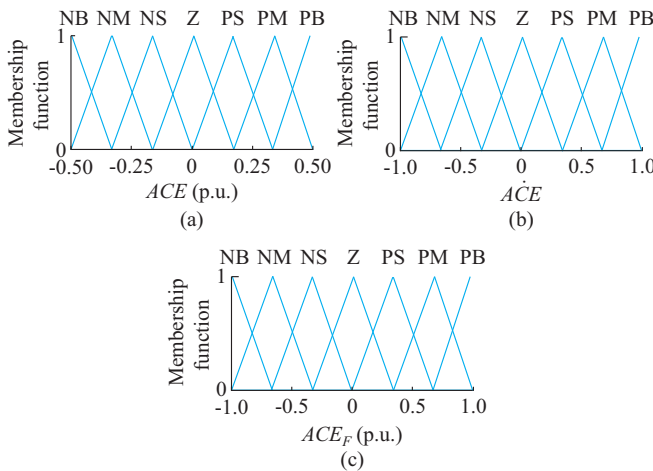| ACE	ACE_F with different $A\dot{C}E$						
	NB	NM	NS	Z	PS	PM	PB
NB	PB	PB	PM	PM	PS	Z	Z
NM	PB	PB	PM	PS	PS	Z	NS
NS	PB	PM	PM	PS	Z	NS	NS
Z	PM	PM	PS	Z	NS	NM	NM
PS	PS	PS	Z	NS	NS	NM	NB
PM	PS	Z	NS	NM	NM	NM	NB
PB	Z	Z	NM	NM	NM	NB	NB

Fig. 2. Membership function for two inputs and one output of fuzzy logic controller. (a) ACE. (b) $A\dot{C}E$. (c) ACE_F.

As shown in Fig. 2, when ACE belongs to PB and $A\dot{C}E$ belongs to PB, which indicates that the frequency deviation is large, the charging/discharging power of BESS belongs to NB at this time, and vice versa. In addition, the output of

fuzzy logic controller is a fuzzy set, which can be defined by the centroid method.

C. Hierarchical Control for BESS

The output signal of fuzzy logic controller fluctuates around zero, which leads to repeated power throughput and reduces the efficiency because of the rapid response ability of the BESS.

In this paper, the hierarchical control includes the BESS management operation and ACE signal state. In the operation control, the entire BESS is divided into two sub-BESSs with the same capacity and power, and only one sub-BESS is charged or discharged at one time. Additionally, considering the capacity limitation, the SOC threshold is limited.

In different ACE signal states, namely the dead zone state, alert state, and crisis state, the ACE signal varies, and thus, the power output should use different control methods. To prevent the excessive throughput, the SOC of BESS is further limited, and the maximum and minimum thresholds are set in this paper. The schematic diagram of hierarchical control is shown in Fig. 3.
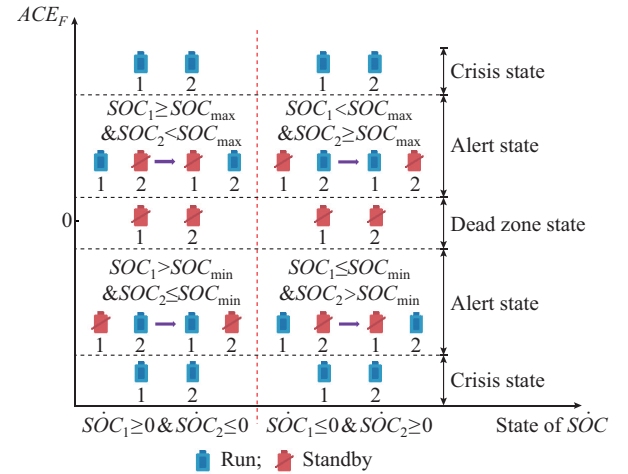

Fig. 3. Schematic diagram of hierarchical control.

1) Dead Zone State

The dead zone state denotes that the magnitude of ACE signal does not reach the set threshold, and the BESS is in the standby state at this time. When there is a small load fluctuation in the power system, the BESS does not work because the ACE signals do not reach the set threshold of dead zone and only the conventional units inject active power through the inertial response. At this time, the ACE deviation is small and does not affect the safe and stable power system operation, as described below.

If $-ACE_F^{dz} \leq ACE_F \leq ACE_F^{dz}$, the response power of BESS is expressed as:

$$\begin{cases} ACE_{E1}^c = ACE_{E1}^{disc} = 0 \\ ACE_{E2}^c = ACE_{E2}^{disc} = 0 \end{cases} \tag{7}$$

2) Alert State

The alert state indicates that the magnitude of ACE signal exceeds the set threshold of dead zone state but does not exceed that of alert state, and the BESS participates in FR

with a coordinated control strategy. In addition, only one sub-BESS is charged or discharged at one time. The response process is described as follows.

1) if $ACE_F > ACE_F^{dz}$ and $S\dot{O}C_1 \geq 0 \& S\dot{O}C_2 \leq 0$, the response power of BESS is expressed as:

$$\begin{cases} ACE_{E1}^c = \min(-ACE_F, P_{E1,\max}^c) \\ ACE_{E2}^c = 0 \end{cases} \tag{8}$$

2) if $ACE_F > ACE_F^{dz}$ and $SOC_1 \geq SOC_{\max} \& SOC_2 < SOC_{\max}$, at this time, the throughput states of the two sub-BESSs need to be switched because the SOC of one sub-BESS reaches the threshold. Thus, the response power of BESS is expressed as:

$$\begin{cases} ACE_{E1}^c = 0 \\ ACE_{E2}^c = \min(-ACE_F, P_{E2,\max}^c) \end{cases} \tag{9}$$

3) if $ACE_F > ACE_F^{dz}$ and $S\dot{O}C_1 \leq 0 \& S\dot{O}C_2 \geq 0$, the response power of BESS is expressed as:

$$\begin{cases} ACE_{E1}^c = 0 \\ ACE_{E2}^c = \min(-ACE_F, P_{E2,\max}^c) \end{cases} \tag{10}$$

4) if $ACE_F > ACE_F^{dz}$ and $SOC_1 < SOC_{\max} \& SOC_2 \geq SOC_{\max}$, the response power of BESS is expressed as:

$$\begin{cases} ACE_{E1}^c = \min(-ACE_F, P_{E1,\max}^c) \\ ACE_{E2}^c = 0 \end{cases} \tag{11}$$

5) if $ACE_F < -ACE_F^{dz}$ and $S\dot{O}C_1 \geq 0 \& S\dot{O}C_2 \leq 0$, the response power of BESS is expressed as:

$$\begin{cases} ACE_{E1}^{disc} = 0 \\ ACE_{E2}^{disc} = \min(-ACE_F, P_{E2,\max}^{disc}) \end{cases} \tag{12}$$

6) if $ACE_F < -ACE_F^{dz}$ and $SOC_1 > SOC_{\min} \& SOC_2 \leq SOC_{\min}$, the same as above, the SOC of one sub-BESS reaches the threshold, and the throughput states of the two sub-BESSs need to be switched. The response power of BESS is expressed as:

$$\begin{cases} ACE_{E1}^{disc} = \min(-ACE_F, P_{E1,\max}^{disc}) \\ ACE_{E2}^{disc} = 0 \end{cases} \tag{13}$$

7) if $ACE_F < -ACE_F^{dz}$ and $S\dot{O}C_1 \leq 0 \& S\dot{O}C_2 \geq 0$, the response power of BESS is expressed as:

$$\begin{cases} ACE_{E1}^{disc} = \min(-ACE_F, P_{E1,\max}^{disc}) \\ ACE_{E2}^{disc} = 0 \end{cases} \tag{14}$$

8) if $ACE_F < -ACE_F^{dz}$ and $SOC_1 \leq SOC_{\min} \& SOC_2 > SOC_{\min}$, the response power of BESS is expressed as:

$$\begin{cases} ACE_{E1}^{disc} = 0 \\ ACE_{E2}^{disc} = \min(-ACE_F, P_{E2,\max}^{disc}) \end{cases} \tag{15}$$

3) Crisis State

The crisis state indicates that the ACE signal magnitude exceeds the alert state set threshold. When a large load fluctuation occurs in the power system, the ACE fluctuates drastically without many active power resources for FR. Thus, the BESS throughput needs to reach the maximum value to ensure the safe and stable operation of the power system, as described below.

If $ACE_F \leq -ACE_F^{em}$ or $ACE_F \geq ACE_F^{em}$, the response power of BESS is expressed as:

$$\begin{cases} ACE_{E1}^c = P_{E1,\max}^c \\ ACE_{E1}^{disc} = P_{E1,\max}^{disc} \\ ACE_{E2}^c = P_{E2,\max}^c \\ ACE_{E2}^{disc} = P_{E2,\max}^{disc} \end{cases} \tag{16}$$

As mentioned above, as the ACE signal value increases, the power signal value received by the BESS gradually increases. However, it also should be noted that the BESS capacity limitations will cause the BESS to do nothing when faced with a large-scale active power shortage. The block of hierarchical control strategy for BESS is shown in Fig. 4.

4) SOC Limiter

The BESS throughput with the control strategy output easily causes the SOC to quickly saturate or run out. Thus, in this paper, a function is used to set the throughput power of BESS, which is not only conductive to making full use of the rapid response capability of BESS but also smoothing the power throughput. Therefore, the real throughput power is obtained as shown in Fig. 5 and (17) and (18). These intervals in the SOC state are expressed as: $[0, SOC_{\min}]$, $[SOC_{\min}, SOC_{low}]$, $[SOC_{low}, SOC_{high}]$, $[SOC_{high}, SOC_{\max}]$, and $[SOC_{\max}, 1]$.

$$\Delta P_E^c = \begin{cases} \min\left(\Delta P_{E,ACE}^c \dfrac{\alpha_1 e^{\frac{\beta_1(SOC_{\max}-SOC)}{SOC_{\max}-SOC_{high}}}}{\phi\left(1+\alpha_1 e^{\frac{\beta_1(SOC_{\max}-SOC)}{SOC_{\max}-SOC_{high}}}\right)}+\varepsilon, P_{E,\max}^c\right) \\ \qquad\qquad\qquad\qquad SOC_{\min} \leq SOC < SOC_{low} \\[4pt] \min(\Delta P_{E,ACE}^c, P_{E1,\max}^c) \\ \qquad\qquad\qquad\qquad SOC_{low} \leq SOC \leq SOC_{high} \\[4pt] \min\left(\Delta P_{E,ACE}^c \dfrac{\alpha_2 e^{\frac{\beta_2(SOC_{\max}-SOC)}{SOC_{\max}-SOC_{high}}}}{\phi\left(1+\alpha_2 e^{\frac{\beta_2(SOC_{\max}-SOC)}{SOC_{\max}-SOC_{high}}}\right)}+\varepsilon, P_{E,\max}^c\right) \\ \qquad\qquad\qquad\qquad SOC_{high} < SOC \leq SOC_{\max} \end{cases} \tag{17}$$

$$\Delta P_E^{disc} = \begin{cases} \min\left(\Delta P_{E,ACE}^{disc} \dfrac{\alpha_2 e^{\frac{\beta_2(SOC-SOC_{\min})}{SOC_{low}-SOC_{\min}}}}{\phi\left(1+\alpha_2 e^{\frac{\beta_2(SOC-SOC_{\min})}{SOC_{low}-SOC_{\min}}}\right)}+\varepsilon, P_{E,\max}^{disc}\right) \\ \qquad\qquad\qquad\qquad SOC_{\min} \leq SOC < SOC_{low} \\[4pt] \min(\Delta P_{E,ACE}^{disc}, P_{E,\max}^{disc}) \\ \qquad\qquad\qquad\qquad SOC_{low} \leq SOC \leq SOC_{high} \\[4pt] \min\left(\Delta P_{E,ACE}^{disc} \dfrac{\alpha_1 e^{\frac{\beta_1(SOC-SOC_{\min})}{SOC_{\max}-SOC_{high}}}}{\phi\left(1+\alpha_1 e^{\frac{\beta_1(SOC-SOC_{\min})}{SOC_{low}-SOC_{\min}}}\right)}+\varepsilon, P_{E,\max}^{disc}\right) \\ \qquad\qquad\qquad\qquad SOC_{high} < SOC \leq SOC_{\max} \end{cases} \tag{18}$$

When the SOC value is low, the BESS has higher charging power and lower discharging power, and vice versa. The SOC control strategy enables the BESS to slowly reach a critical state and give full play to its advantages.
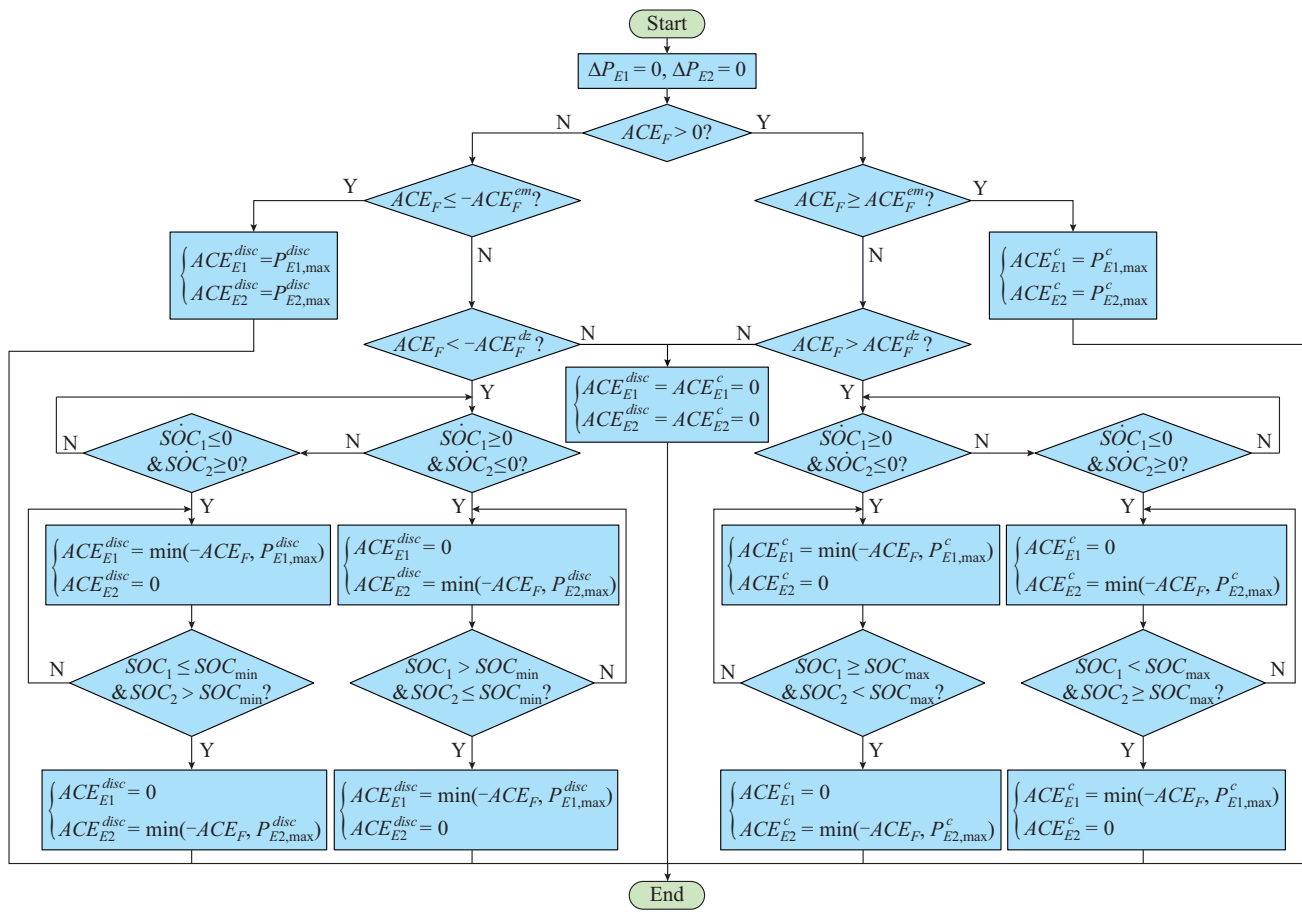
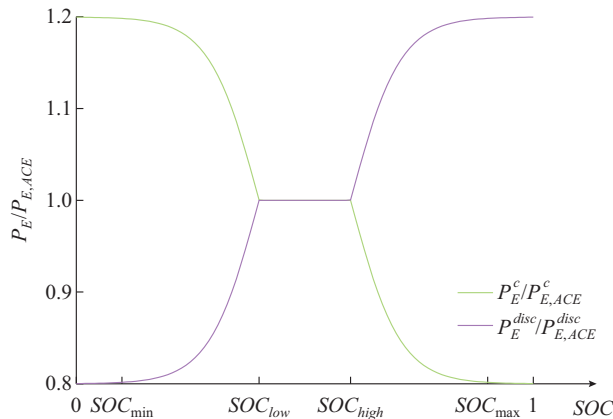Fig. 4.   Block of hierarchical control strategy for BESS.

Fig. 5.   Real throughput power.

III. COMPREHENSIVE ASSESSMENT OF BESS IN FR CONSIDERING ACE RISK AND COST

The effect of power system stability can be improved by utilizing BESSs. However, the establishment of BESS leads to a substantial increase in the FR cost. To evaluate the FR cost comprehensively, this paper considers the influence of multiple factors, including the ACE risk, life loss of BESS, throughput conversion times, and BESS utilization. The ACE risk and other parameters are obtained through an analysis of the simulation results. Then, the optimal DOD is

solved according to the proposed evaluation model, and the DOD is substituted into the coordinated control strategy to obtain the optimal control result.

A. ACE Risk

ACE risk represents the degree of influence of ACE deviation on the system risk and economic loss. ACE deviation determines the ACE risk, and the greater the deviation, the greater the risk. In addition, ACE risk creates certain economic losses in the power system, and the greater the loss, the greater the risk. The exponential function $h(\Delta ACE)$ is used to evaluate the risk caused by ACE deviation, as described below [33]:

$$h(\Delta ACE) = c e^{\mu |\Delta ACE|} \tag{19}$$

Formula (20) expresses the degree of influence of the ACE deviation on the power system risk. Set $g(|\Delta ACE|)$ as the ACE distribution function, and the power system risk caused by ACE deviation is formulated as:

$$q(\Delta ACE) = \int g(|\Delta ACE|) h(|\Delta ACE|) d|\Delta ACE| \tag{20}$$

B. Life Loss of BESS

The BESS operation has life loss, which is reflected by the number of charging/discharging cycles and determined by the DOD. In general, the smaller the DOD, the smaller the life loss, and vice versa. Therefore, for a charging/discharging cycle with a given range of DODs, the life loss of

BESS can be described as [34], [35]:

$$L_{life}(DOD) = N \cdot DOD^{-\delta} \tag{21}$$

$$L_{loss} = \sum \frac{1}{L_{life}(DOD)} = \sum \frac{1}{N \cdot DOD^{-\delta}} \tag{22}$$

C. Throughput Conversion Times and BESS Utilization

The repeated charging/discharging leads to the life loss of BESS. However, it is much smaller than the loss by power throughput. The throughput conversion times are realized by data fitting in this paper. In addition, a higher DOD increases the BESS life loss, while a smaller DOD reduces the FR effect. The BESS utilization u is described as:

$$u = \frac{1}{DOD} \tag{23}$$

Therefore, the objective of the model is minimizing the FR cost caused by BESS, and the optimization variable is the DOD. The objective function is illustrated in (24). The solution method is the traversing method.

$$\min \ F_{cost}(\Delta ACE, DOD) = q(\Delta ACE) + L_{loss}Wu + \gamma B_{con} =$$
$$q(\Delta ACE) + \sum W \frac{1}{N \cdot DOD^{-\delta}} \frac{1}{DOD} + \gamma B_{con} \tag{24}$$

IV. CASE STUDY

A. Simulation Model

The two-area system model is shown in Fig. 1. FR is achieved through conventional units and BESS in this power system. The base power of the power system is set to be 10 GW, and the base frequency is 50 Hz. The rated power and rated capacity of the BESS are 200 MW and 5 MWh, respectively. In this case study, random load fluctuation signal ΔP_{L1} in a time series is assumed to be added at area 1, and ΔP_{L2} is set to be zero, as shown in Fig. 6. Moreover, relevant parameters are shown in Tables II and III.
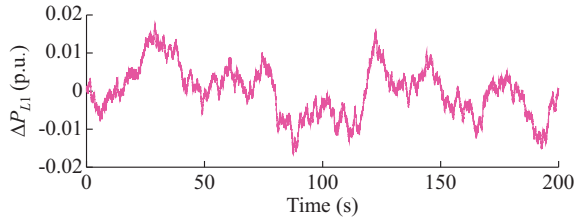

Fig. 6.   Random load fluctuation.

TABLE II
PARAMETERS OF POWER SYSTEM MODEL

Parameter	Value	Parameter	Value
M_1, M_2 (MW·s/Hz)	10	R_1, R_2 (Hz/MW)	0.05
D_1, D_2 (MW/Hz)	1	K_{I1}, K_{I2}	0.822
T_{G1}, T_{G2}	0.08	K_{P1}, K_{P2}	0.16
T_{RH1}, T_{RH2}	10	B_1, B_2 (MW/Hz)	21
T_{CH1}, T_{CH2}	0.3	β_1, β_2	0.2
F_{HP1}, F_{HP2}	0.5	T_{tie}	10
ACE_F^{dz} (p.u.)	0.00167	ACE_F^{em} (p.u.)	0.005

TABLE III
PARAMETERS OF BESS MODEL

Parameter	Value	Parameter	Value
T_{E1}, T_{E2} (s)	0.02	η_c, η_{disc} (%)	95
$P_{E1, max}^c, P_{E2, max}^c$ (p.u.)	0.02	$P_{E1, max}^{disc}, P_{E2, max}^{disc}$ (p.u.)	0.02
SOC_{min}	0.1	SOC_{low}	0.4
SOC_{high}	0.6	SOC_{max}	0.9
α_1 (%)	0.0285	α_2 (%)	1.11
ϕ	6.8	ε	0.8
c	600	μ	400
N	1591	δ	2.09

B. Simulations of FR

To validate the control strategy, two different scenarios are presented.

1) Scenario 1: Control Effects with Different Strategies

Four strategies are set in this scenario, which determines the validity of the proposed control strategy by comparing the range of ACE deviation among different strategies: ① strategy A: FR by conventional units and sub-BESSs with coordinated control strategy (the control strategy proposed in this paper); ② strategy B: FR by conventional units and co-ordinated control for hybrid energy storage system [22]; ③ strategy C: FR by conventional units and the whole BESS with drop control strategy; ④ strategy D: FR by conventional units and the whole BESS with the proportional integral (PI) control strategy ($K_P = 0.5, K_I = -0.005$).

The power changes, frequency signal changes, and ACE signal deviation with different strategies can be observed in Figs. 7-9, respectively.
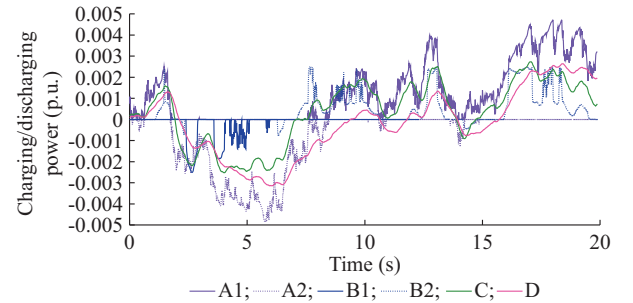

Fig. 7.   Charging/discharging power with different strategies under random disturbance.
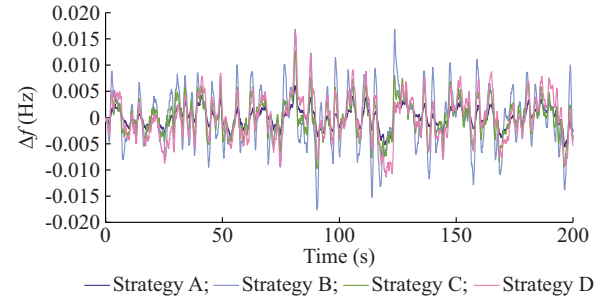

Fig. 8.   Frequency deviation with different strategies.

As shown in Fig. 7, A1 and A2 are the power changes of

two sub-BESSs in 20 s; B1 and B2 are the power changes of two energy storage systems. Compared with other control strategies, the fuzzy logic controller (strategy A) has a higher response accuracy and can accurately track the change in ACE signals, which proves the superiority of fuzzy logic controller.

As shown in Fig. 8, the frequency deviation range of the strategy A is smaller than that of the other strategies, which proves the effectiveness of this strategy. It clearly shows that the effect of FR with strategy A is better than those with other strategies, which proves that the proposed control strategy improves the stability of the power system. In addition, it further proves that the rapid response of BESS can be fully utilized by a reasonable control method.
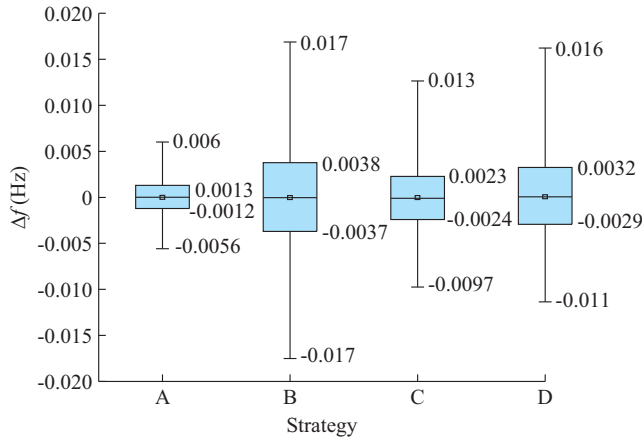

Fig. 10.   Throughput power of two sub-BESSs.

Fig. 11.   SOC of BESS with different strategies.

Fig. 9.   Boxplot of ACE deviation with different strategies.

As shown in Fig. 9, the ranges of the maximum ACE deviation with strategies A-D are [−0.005 p.u., 0.0036 p.u.], [−0.0079 p.u., 0.0104 p.u.], [−0.0063 p.u., 0.0097 p.u.], and [−0.0119 p. u., 0.0129 p. u.], respectively. In other words, compared with strategies B, C, and D, the range of the maximum ACE deviation with strategy A is decreased by 53%, 39%, and 56.3%, respectively.

At the same time, the ranges of the main ACE deviation with strategies A-D are [−0.0009 p. u., 0.0011 p. u.], [−0.0023 p. u., 0.0029 p.u.], [−0.0015 p.u., 0.0017 p.u.], and [−0.0021 p.u., 0.0025 p. u.], respectively. In other words, compared with strategies B, C, and D, the range of the main ACE deviation with strategy A is decreased by 59.8%, 34.7%, and 54.6%, respectively. According to the above description, it is known that through the proposed coordinated control strategy, the FR with BESS is beneficial for decreasing the oscillation and overshot, and strengthening the stability of the power system.

In addition, strategy A also reduces the throughput conversion times, and its throughput power and SOC curve are shown in Figs. 10 and 11, respectively.

As shown in Fig. 10, only one sub-BESS can be charged and discharged at the same time with strategy A. Simultaneously, this strategy decreases the throughput conversion times from 73 to 5, as shown in Table IV. However, as the ACE deviation range shrinks and the throughput conversion times decrease, BESS life loss also changes accordingly, as shown in Table IV.
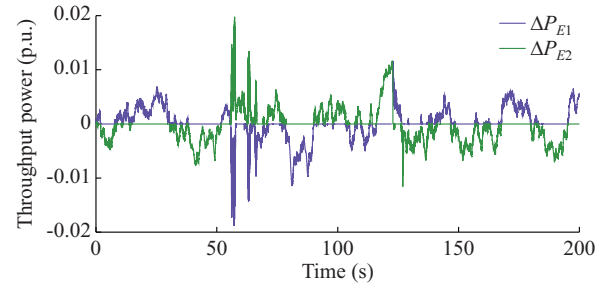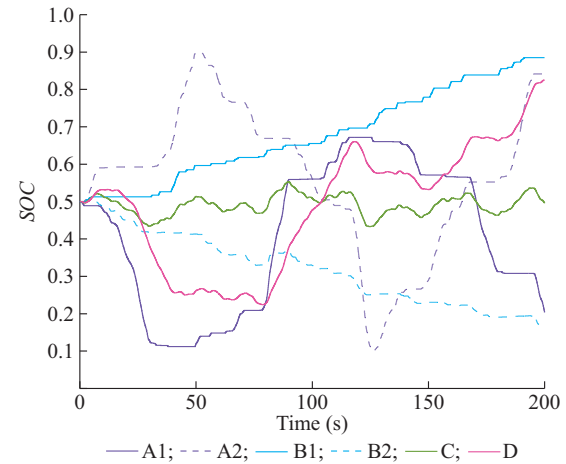
TABLE IV
THROUGHPUT CONVERSION TIMES AND LIFE LOSS IN SCENARIO 1

Strategy	B_{con}	L_{loss} (%)
A	5	0.12000
B	50	0.00923
C	73	0.00188
D	47	0.01769

The power system stability is improved by strategy A, however, the life loss of BESS increases by at least 13 times, which affects the operation and economy of the BESS.

2) Scenario 2: Life Loss with Different Throughput Thresholds

The improvement in FR reduces the BESS running time and therefore decreases the BESS life loss by limiting its SOC threshold. Four methods based on strategy A are set in this scenario to verify the impact of the throughput threshold on life loss: ① method a: the threshold range of SOC is set to be [0.1, 0.9]; ② method b: the threshold range of SOC is set to be [0.2, 0.8]; ③ method c: the threshold range of SOC is set to be [0.3, 0.7]; ④ method d: the threshold range of SOC is set to be [0.4, 0.6]. The SOC curves of two sub-BESSs with four methods are shown in Fig. 12.

Based on the same control strategy, the effect of FR is almost the same with the four threshold ranges. As shown in Fig. 12, with the decrease in the threshold range, the number of throughput conversion times increases, and the SOC fluctuation becomes more severe. In addition, if the disturbance is large, the two sub-BESSs are charged or discharged fully.

However, when the BESS stops working, the effect of FR will be worse than the other threshold ranges. Therefore, the capacity of the BESS needs to be considered when setting the throughput threshold range. Simultaneously, the life losses and the throughput conversion times of BESS with different throughput threshold ranges are shown in Table V.
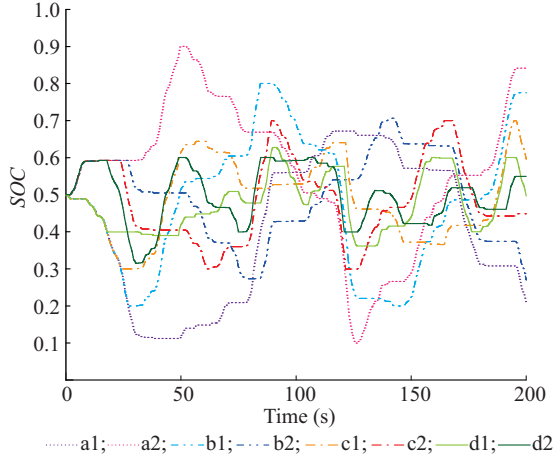

Fig. 12.   SOC of two sub-BESSs with different threshold ranges.

TABLE V
LIFE LOSSES AND THROUGHPUT CONVERSION TIMES IN SCENARIO 2

Method	B_{con}	L_{loss} (%)
a	4	0.1200
b	13	0.0595
c	20	0.0534
d	36	0.0324

Fig. 13.   Changing trend in the optimal DOD.

Fig. 14.   Optimized SOC of BESS.

In Table V, when the threshold range is reduced, the throughput conversion times increase gradually; however, the life loss of BESS is curtailed. This also verifies that the shallow throughput strategy is better than the deep throughput.

3) Quantitative Evaluation of Different BESS Strategies

For the overall evaluation of the effectiveness of the FR strategy proposed in this paper, the evaluation indicators proposed in this section are used. Through analyzing this indicator, it can be found that strategy A has the lowest FR cost. In addition, to analyze the impact of the cost and penalty coefficient on the optimal DOD, Fig. 13 shows the changing trend in the optimal DOD with different costs and penalty coefficients, and the optimized SOC of BESS is shown in Fig. 14.

It is noted that the optimal DOD is 0.39 in Fig. 13, which means that the throughput threshold range is [0.305, 0.695]. It is also reported that the optimal DOD decreases constantly when the penalty coefficient is reduced, while the optimal DOD increases when the BESS costs increase. This proves again that when the BESS cost continues to decrease, the range of available DOD becomes larger. As shown in Fig. 14, the upper and lower thresholds of SOC of BESS are 0.695 and 0.305, respectively, and the DOD is the threshold difference of the SOC, which is 0.39. Therefore, the DOD of BESS is always at the optimal value, which is controlled by the SOC thresholds and has nothing to do with the fluctuation in the ACE.
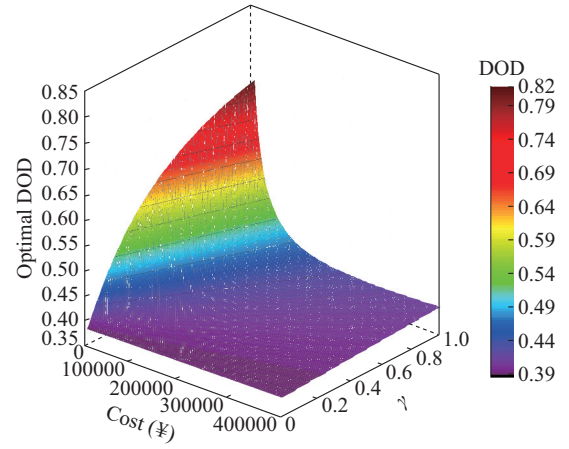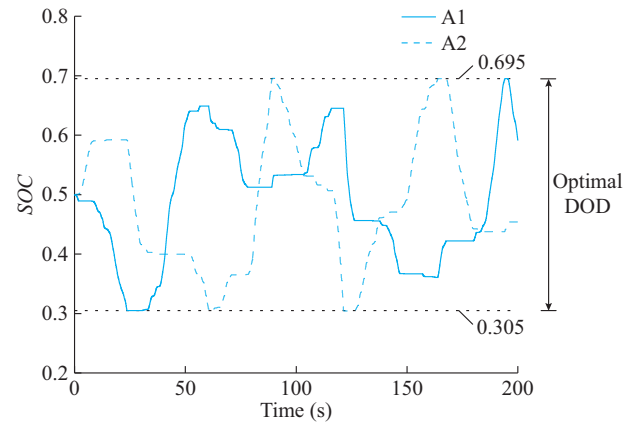
V. CONCLUSION

This paper proposes a methodology based on fuzzy logic and hierarchical controllers for enhancing the FR effectiveness. Compared with other strategies such as coordinated control, traditional drop control, and PI control, the maximum and central ACE deviation ranges decrease by at least 39% and 34.7%, respectively. Through the hierarchical control, repeated charging/discharging of BESS is avoided. To achieve a balance between the ACE reduction and operational economy to reduce the life loss of BESS, this paper proposes a comprehensive evaluation method of the FR effect. The optimal DOD of BESS is 0.39 in our study case, i. e., the throughput threshold range is [0.305, 0.695]. Furthermore, the control strategy can be generalized to other types of energy storage devices, achieving better effects with a further reduction in energy storage cost.

REFERENCES

[1] T. P. Teixeira and C. L. T. Borges, "Operation strategies for coordinating battery energy storage with wind power generation and their effects on system reliability," *Journal of Modern Power Systems and Clean Energy*, vol. 9, no. 1, pp. 190-198, Jan. 2021.

[2] Y. Ye, Y. Qiao, and Z. Lu, "Revolution of frequency regulation in the converter-dominated power system," *Renewable and Sustainable Energy Reviews*, vol. 111, pp. 145-156, Sept. 2019.

[3] F. R. Islam, A. Lallu, K. A. Mamun *et al.*, "Power quality improvement of distribution network using BESS and capacitor bank," *Journal of Modern Power Systems and Clean Energy*, vol. 9, no. 3, pp.

625-632, Mar. 2021.

[4] K. Doenges, I. Egido, L. Sigrist *et al.*, "Improving AGC performance in power systems with regulation response accuracy margins using battery energy storage system (BESS)," *IEEE Transactions on Power Systems*, vol. 35, no. 4, pp. 2816-2825, Jul. 2020.

[5] K. S. El-Bidairi, H. D. Nguyen, T. S. Mahmoud *et al.*, "Optimal sizing of battery energy storage systems for dynamic frequency control in an islanded microgrid: a case study of Flinders Island, Australia," *Energy*, vol. 195, no. 1, pp. 117059, Mar. 2020.

[6] X. Xu, M. Bishop, O. Donna G *et al.*, "Application and modeling of battery energy storage in power systems," *CSEE Journal of Power and Energy Systems*, vol. 2, no. 3, pp. 82-90, Sept. 2016.

[7] U. Akram, M. Nadarajah, R. Shah *et al.*, "A review on rapid responsive energy storage technologies for frequency regulation in modern power systems," *Renewable and Sustainable Energy Reviews*, vol. 120, pp. 1-18, Mar. 2020.

[8] X. Dong, Y. Zhang, and T. Jiang, "Planning-operation co-optimization model of active distribution network with energy storage considering the lifetime of batteries," *IEEE Access*, vol. 6, pp. 59822-59832, Oct. 2018.

[9] M. H. Marzebali, M. Mazidi, and M. Mohiti, "An adaptive droop-based control strategy for fuel cell-battery hybrid energy storage system to support primary frequency in stand-alone microgrids," *Journal of Energy Storage*, vol. 27, pp. 1-16, Feb. 2020.

[10] H. Zhao, M. Hong, W. Lin *et al.*, "Voltage and frequency regulation of microgrid with battery energy storage systems," *IEEE Transactions on Smart Grid*, vol. 10, no. 1, pp. 414-424, Aug. 2019.

[11] J. W. Shim, G. Verbic, H. Kim *et al.*, "On droop control of energy-constrained battery energy storage systems for grid frequency regulation," *IEEE Access*, vol. 7, pp. 166353-166364, Nov. 2019.

[12] N. Sockeel, J. Gafford, B. Papari *et al.*, "Virtual inertia emulator-based model predictive control for grid frequency regulation considering high penetration of inverter-based energy storage system," *IEEE Transactions on Sustainable Energy*, vol. 11, no. 4, pp. 2932-2939, Mar. 2020.

[13] H. Liu, K. Huang, N. Wang *et al.*, "Optimal dispatch for participation of electric vehicles in frequency regulation based on area control error and area regulation requirement," *Applied Energy*, vol. 240, pp. 46-55, Apr. 2019.

[14] W. Jin, Y. Shin, and M. Kim, "Hybrid operation strategy of wind energy storage system for power grid frequency regulation," *IET Generation, Transmission & Distribution*, vol. 10, no. 3, pp. 736-749, Feb. 2016.

[15] B. Li, X. M, and B. Chen, "Direct control strategy of real-time tracking power generation plan for wind power and battery energy storage combined system," *IEEE Access*, vol. 7, pp. 147169-147178, Oct. 2019.

[16] S. Zhang, Y. Mishra, and M. Shahidehpour, "Fuzzy-logic based frequency controller for wind farms augmented with energy storage systems," *IEEE Transactions on Power Systems*, vol. 31, no. 2, pp. 1595-1603, May 2016.

[17] J. Boyle, T. Littler, and A. Foley, "Battery energy storage system state-of-charge management to ensure availability of frequency regulating services from wind farms," *Renewable Energy*, vol. 160, pp. 1119-1135, Nov. 2020.

[18] P. Iurilli, C. Brivio, and M. Merlo, "SoC management strategies in battery energy storage system providing primary control reserve," *Sustainable Energy, Grids and Networks*, vol. 19, pp. 1-11, Sept. 2019.

[19] Z. Tan, X. Li, L. He *et al.*, "Primary frequency control with BESS considering adaptive SoC recovery," *International Journal of Electrical Power & Energy Systems*, vol. 117, pp. 1-12, May 2020.

[20] U. Akram and M. Khalid, "A coordinated frequency regulation framework based on hybrid battery-ultracapacitor energy storage technologies," *IEEE Access*, vol. 6, pp. 7310-7320, Dec. 2018.

[21] H. Jia, X. Li, Y. Mu *et al.*, "Coordinated control for EV aggregators and power plants in frequency regulation considering time-varying delays," *Applied Energy*, vol. 210, pp. 1363-1376, Jan. 2018.

[22] J. Zhong, L. He, C. Li *et al.*, "Coordinated control for large-scale EV charging facilities and energy storage devices participating in frequency regulation," *Applied Energy*, vol. 123, pp. 253-262, Jun. 2014.

[23] S. P. Melo, U. Brand, T. Vogt *et al.*, "Primary frequency control provided by hybrid battery storage and power-to-heat system," *Applied Energy*, vol. 233-234, pp. 220-231, Jan. 2019.

[24] M. M. Islam, X. Zhong, Z. Sun *et al.*, "Real-time frequency regulation using aggregated electric vehicles in smart grid," *Computers & Industrial Engineering*, vol. 134, pp. 11-26, Aug. 2019.

[25] M. U. Jan, A. Xin, M. A. Abdelbaky *et al.*, "Adaptive and fuzzy pi controllers design for frequency regulation of isolated microgrid integrated with electric vehicles," *IEEE Access*, vol. 8, pp. 87621-87632, May 2020.

[26] P. Li, Z. Tan, Y. Zhou *et al.*, "Secondary frequency regulation strategy with fuzzy logic method and self-adaptive modification of state of charge," *IEEE Access*, vol. 6, pp. 43575-43585, Jul. 2018.

[27] J. Li, R. Xiong, H. Mao *et al.*, "Design and real-time test of a hybrid energy storage system in the microgrid with the benefit of improving the battery lifetime," *Applied Energy*, vol. 218, pp. 470-478, Mar. 2018.

[28] D.-I. Stroe, V. Knap, M. Swierczynski *et al.*, "Operation of a grid-connected lithium-ion battery energy storage system for primary frequency regulation: a battery lifetime perspective," *IEEE Transactions on Industry Applications*, vol. 53, no. 1, pp. 430-438, Oct. 2017.

[29] B. Lian, A. Sims, D. Yu *et al.*, "Optimizing LiFePO$_4$ battery energy storage systems for frequency response in the UK system," *IEEE Transactions on Sustainable Energy*, vol. 8, no. 1, pp. 385-394, Aug. 2017.

[30] M. Arifujjaman, "A comprehensive power loss, efficiency, reliability and cost calculation of a 1 MW/500 kWh battery based energy storage system for frequency regulation application," *Renewable Energy*, vol. 74, pp. 158-169, Feb. 2015.

[31] X. Han, Z. Wei, Z. Hong *et al.*, "Adaptability assessment method of energy storage working conditions based on cloud decision fusion under scenarios of peak shaving and frequency regulation," *Journal of Energy Storage*, vol. 32, pp. 101784, Dec. 2020.

[32] J. Marchrraber, W. Gawlik, G. Wailzer *et al.*, "Reducing SoC-management and losses of battery energy storage systems during provision of frequency containment reserve," *Journal of Energy Storage*, vol. 27, pp. 1-10, Feb. 2020.

[33] J. Wu, Y. Qiao, Z. Lu *et al.*, "Coordinated operation strategy of hybrid storage system in wind power peak shaving scenarios," *The Journal of Engineering*, vol. 2017, no. 13, pp. 1254-1258, Nov. 2017.

[34] J. Li, A. M. Gee, M. Zhang *et al.*, "Analysis of battery lifetime extension in a SMES-battery hybrid energy storage system using a novel battery lifetime model," *Energy*, vol. 86, pp. 175-185, Jun. 2015.

[35] J. Wang, P. Liu, J. Hicks-Garner *et al.*, "Cycle-life model for graphite-LiFePO$_4$ cells," *Journal of Power Sources*, vol. 196, no. 8, pp. 3942-3948, Apr. 2011.

Kaifeng Wang received the B.E. degree in automation from Changzhou Institute of Technology, Changzhou, China, in 2018. He is currently pursuing his M.S. degree in control science and engineering in Xinjiang University, Urumqi, China. His research interests include renewable energy and power system security and control.

Ying Qiao received the B.E. degree in electrical engineering from Shanghai Jiao Tong University, Shanghai, China, in 2002, and the Ph.D. degree in electrical engineering from Tsinghua University, Beijing, China, in 2008. She is currently working as an Assistant Professor in Tsinghua University. Her research interests include renewable energy and power system security and control.

Lirong Xie received the B.E. degree in electrical engineering from Xinjiang University, Urumqi, China, in 1992, the M.S. degree in control science and engineering from Dalian University of Technology, Dalian, China, in 2004. She is currently working as a Professor in Xinjiang University, Urumqi, China. Her research interests include renewable energy and control system optimization.

Jiaming Li received the B.E. degree in electrical engineering from Tsinghua University, Beijing, China, in 2019. He is currently pursuing the Ph.D. degree in Electrical Engineering from Tsinghua University. His research interests include energy storage planning and operation and the application of artificial intelligence & big data technology in power system.

Zongxiang Lu received the B.E. and Ph.D. degrees in electrical engineering from Tsinghua University, Beijing, China, in 1998 and 2002, respectively. He is currently working as an Assistant Professor in Tsinghua University, Beijing, China. His research interests include large-scale wind power/PV stations integration analysis and control, energy and electricity strategy planning, power system reliability, DG, and microgrid.

Huan Yang received the B.E. degree in automation from Xi'an Aeronautical University, Xi'an, China, in 2017. He is currently pursuing the M.S. degree in control science and engineering in Xinjiang University, Urumqi, China. His research interests include renewable energy and electricity market.